T18196 9 S0 (1)

SANDIA REPORT

SANDIA REPORT

SAND96-8250 • UC-406
Unlimited Release
Printed July 1996

Buoyant Instabilities in Downward Flow in a Symmetrically Heated Vertical Channel

G. H. Evans, R. Greif

Prepared by
Sandia National Laboratories
Albuquerque, New Mexico 87185 and Livermore, California 94550
for the United States Department of Energy
under Contract DE-ACO4-94AL85000

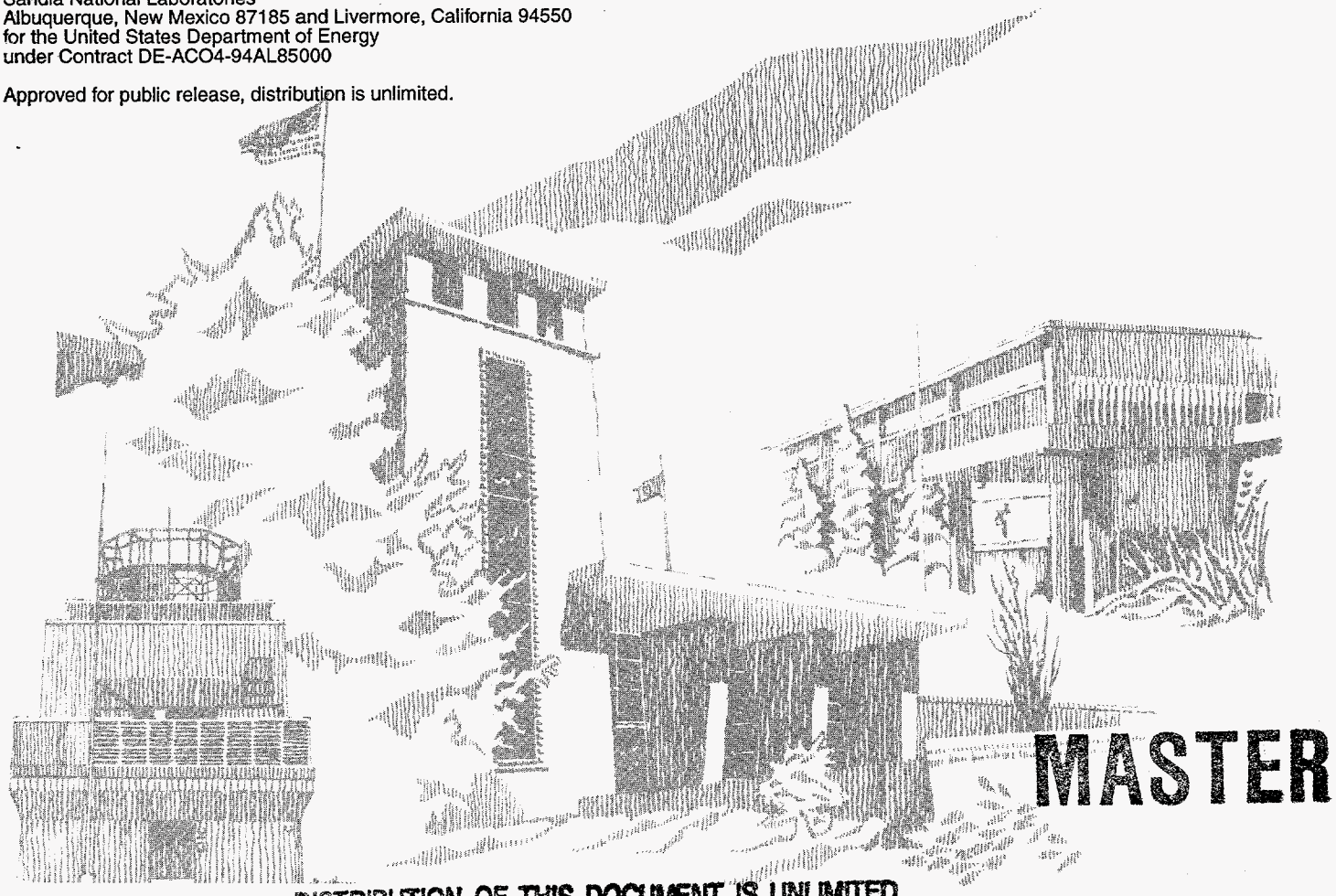

Issued by Sandia National Laboratories, operated for the United States Department of Energy by Sandia Corporation.

UC-406

SAND96-8250
Unlimited Release
Printed July 1996

Buoyant Instabilities in Downward Flow in a Symmetrically Heated Vertical Channel

G. Evans
Thermal and Plasma Processes Department
Sandia National Laboratories, Livermore, CA 94550

R. Greif
Mechanical Engineering Department
University of California, Berkeley, CA 94720

ABSTRACT

This study of the downward flow of nitrogen in a tall, partially heated vertical channel (upstream isothermal at T_{in}^*, heated region isothermal at T_s^*, downstream adiabatic) shows the strong effects of buoyancy even for small temperature differences. Time-dependent oscillations including periodic flow reversals occur along the channel walls. Although the flow and heat transfer are asymmetric, the temperature and axial component of velocity show symmetric reflections at two times that are half a period apart and the lateral component of velocity shows antisymmetric reflections at the two times. There is strong interaction between the downward flow in the central region of the channel and the upward flow along the heated channel walls. At the top of the heated region, the upward buoyant flow turns toward the center of the channel and is incorporated into the downward flow. Along the channel centerline there are nonmonotonic variations of the axial component of velocity and temperature and a large lateral component of velocity that reverses direction periodically. Results are presented for Re=219.7 and Gr/Re^2=1.83, 8.0, and 13.7. The heat transfer and the frequency of the oscillations increases and the flow and temperature fields become more complex as Gr/Re^2 increases. The results have applications to fiber drying, food processing, crystal growth, solar energy collection, cooling of electronic circuits, ventilation, etc.

NOMENCLATURE

Gr	Grashof number, $g(T_s^* - T_{in}^*)W^{*3}/(T_{in}^* \nu_{in}^{*2})$
Gr/Re^2	mixed convection parameter, $g(T_s^* - T_{in}^*)W^*/(T_{in}^* u_{in}^{*2})$
L	dimensionless length of heated region, $L = L^*/w^* = 8.6$
Nu	local Nusselt numbers, $-k\frac{\partial T}{\partial y}\|_{y=0}$, $k\frac{\partial T}{\partial y}\|_{y=1}$
Nu_{avg}	spatially averaged Nusselt numbers, $1/L \int_0^L Nu \Delta x$
Pr	Prandtl number, $c_{p_{in}}^* \mu_{in}^*/k_{in}^*$
Re	Reynolds number, $\rho_{in}^* u_{in}^* w^*/\mu_{in}^*$
T	temperature, $(T^* - T_{in}{}^*)/(T_s{}^* - T_{in}{}^*)$
c_p	specific heat
g	acceleration of gravity
k	thermal conductivity
p_m	motion pressure
t	time
u	axial component of velocity
u_{in}^*	average inlet velocity (cm/s)
v	lateral component of velocity
w^*	channel width (cm)
x	axial coordinate
y	lateral coordinate

Greek symbols

ρ	density
μ	dynamic viscosity
ν	kinematic viscosity

Subscripts and superscripts

in	evaluated at channel inlet
s	at channel surfaces
*	dimensional quantity

INTRODUCTION

Buoyant effects in fluid flow in vertical tubes or channels are common and have been studied extensively (Ostrach [1]; Morton [2]; Scheele and Hanratty [3]; Lawrence and Chato [4]; Zeldin and Schmidt [5]; Quintiere and Mueller [6]; Cebeci et al. [7]; Yao [8]; Shadday [9]; Habchi and Acharya [10]; Wang et al. [11]). Recently, the time-dependent and asymmetric opposed mixed convection flow in a vertical channel with specified heat flux conditions has been studied numerically for low Pr (Chang and Lin [12]) and for Pr=0.72 and 7.0 (Lin et al. [13]). Other studies concerning the unstable nature of opposed flow mixed convection have been made by Guerrero and Hart [14]; Rogers and Yao [15]; Joye and Jacobs [16]; and Gau et al. [17].

In [15], nonlinear instability analysis was used to predict flow instability in both aiding and opposing mixed convection in a vertical tube with a linearly varying wall temperature profile. For aiding flow the heat transfer predicted from the single wave theory is smaller than what is observed; for Re=600, the predicted heat transfer is increased by considering multiple waves. In [16], periodic temperature oscillations in opposed flow mixed convection in water in a partially heated (isothermal) vertical tube were measured upstream of the start of the heated region for Re=600 and $Gr=5x10^7$; the heat transfer was shown to lie along a forced convection asymptote for Re<2000. In [17], temperature fluctuations and unstable flow of air were observed in opposed flow mixed convection in a vertical heated converging channel (one wall constant heat flux, the other insulated) for $Gr/Re^2=40$ (where Gr is based on the heat flux) and Re=250; for a parallel plate channel the heat transfer was correlated with two different expressions depending on the range of Gr/Re^2.

In Lin et al. [13], the cold downward forced flow first passed through an insulated region before entering the constant heat flux region; time variations of the average heat transfer, the axial component of velocity, and the temperature at two axial locations in the middle and at the downstream ends of the constant heat flux region were presented for Gr/Re^2 up to 4. In some applications a cold section is located above the heated region. The effects of different thermal boundary conditions above the heated region are important since strong buoyancy causes the fluid flow to move upward along the heated surface. This effect is more pronounced at strong buoyancy as shown in this study.

The results for the axial and lateral profiles of both velocity components and temperature and axial profiles of the heat transfer show the asymmetric nature of the phenomena as well as symmetric reflections at times that are half a period apart. The results exhibit nonmono-

tonic variations of the axial component of velocity and temperature and a large lateral component of velocity along the channel centerline. These effects can occur in practice for small temperature differences. The results have applications to fiber drying, food processing, crystal growth, solar energy collection, electronic circuit cooling, ventilation, etc. For example, in fiber drying, the opposed flow instabilities give rise to low frequency oscillations which can lead to lateral fiber motion and fiber tangling and breakage.

ANALYSIS

The geometry of the system is shown in Figure 1. Nitrogen at atmospheric pressure and 300 K flows downward in a vertical channel with walls maintained at 300 K for $x<0$. At $x=0$ the downward flow encounters a second region of the channel ($0\leq x<8.6$) that is at an elevated temperature, T_s^*. Beyond the second region ($x\geq 8.6$) the gas flows through a final region of the channel that is adiabatic. The problem is symmetric about the centerline of the channel ($y=0.5$). At the inlet ($x=-4.3$), the velocity distribution is parabolic. The section above the heated (isothermal at T_s^*) region serves two purposes: first, it allows the inlet boundary conditions to be applied where the flow is unidirectional, and second, the effects of a cold surface above a hot zone on the rising, heated buoyant flow can be determined.

In the adiabatic region below the heated region, the flow returns to the unidirectional condition before exiting the channel. The two-dimensional, planar, dimensionless equations for the flow of a single component gas at low Mach number are:

$$\frac{\partial \rho}{\partial t} + \frac{\partial (\rho u)}{\partial x} + \frac{\partial (\rho v)}{\partial y} = 0 \tag{1}$$

$$\frac{\partial (\rho u)}{\partial t} + \frac{\partial}{\partial x}\left(\rho uu - \frac{\mu}{\mathrm{Re}}\frac{\partial u}{\partial x}\right) + \frac{\partial}{\partial y}\left(\rho vu - \frac{\mu}{\mathrm{Re}}\frac{\partial u}{\partial y}\right) = -\frac{\partial p_m}{\partial x} - \frac{\mathrm{Gr}}{\mathrm{Re}^2}\frac{T}{[1+T(T_s^*/T_{\mathrm{in}}^* - 1)]}$$
$$+ \frac{1}{\mathrm{Re}}\frac{\partial}{\partial x}\left[\mu\frac{\partial u}{\partial x} - \frac{2\mu}{3}\left(\frac{\partial u}{\partial x} + \frac{\partial v}{\partial y}\right)\right] + \frac{1}{\mathrm{Re}}\frac{\partial}{\partial y}\left(\mu\frac{\partial v}{\partial x}\right) \tag{2}$$

$$\frac{\partial (\rho v)}{\partial t} + \frac{\partial}{\partial x}\left(\rho uv - \frac{\mu}{\mathrm{Re}}\frac{\partial v}{\partial x}\right) + \frac{\partial}{\partial y}\left(\rho vv - \frac{\mu}{\mathrm{Re}}\frac{\partial v}{\partial y}\right) = -\frac{\partial p_m}{\partial y}$$
$$+ \frac{1}{\mathrm{Re}}\frac{\partial}{\partial y}\left[\mu\frac{\partial v}{\partial y} - \frac{2\mu}{3}\left(\frac{\partial u}{\partial x} + \frac{\partial v}{\partial y}\right)\right] + \frac{1}{\mathrm{Re}}\frac{\partial}{\partial x}\left(\mu\frac{\partial u}{\partial y}\right) \tag{3}$$

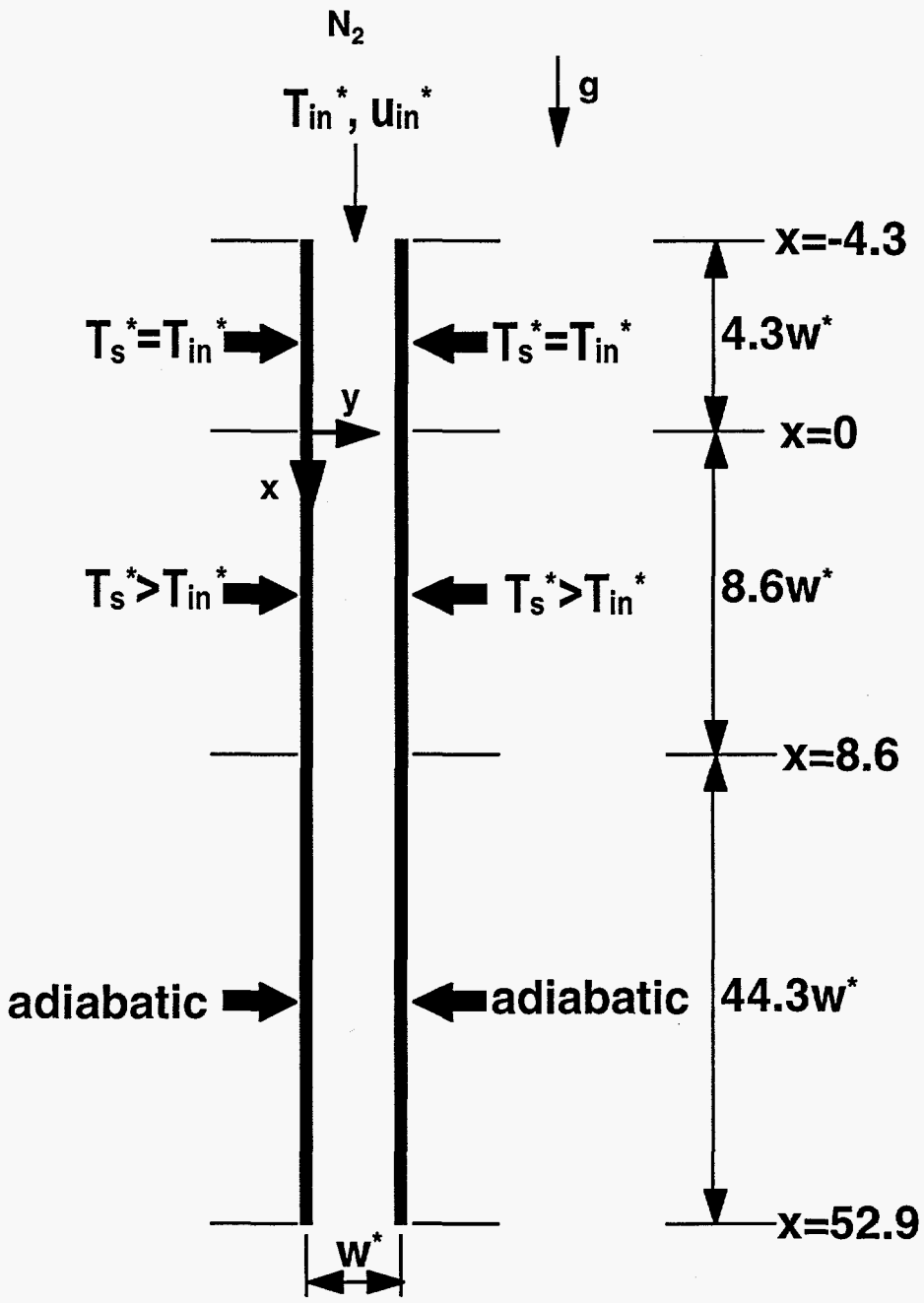

Figure 1. Geometry (not to scale) and boundary conditions.

$$\frac{\partial(\rho T)}{\partial t}+\frac{\partial}{\partial x}\left(\rho uT-\frac{1}{\mathrm{Re}\cdot\mathrm{Pr}}\frac{k}{c_p}\frac{\partial T}{\partial x}\right)+\frac{\partial}{\partial y}\left(\rho vT-\frac{1}{\mathrm{Re}\cdot\mathrm{Pr}}\frac{k}{c_p}\frac{\partial T}{\partial y}\right)=$$

$$\frac{1}{\mathrm{Re}\cdot\mathrm{Pr}}\frac{k}{{c_p}^2}\left(\frac{\partial T}{\partial x}\frac{\partial c_p}{\partial x}+\frac{\partial T}{\partial y}\frac{\partial c_p}{\partial y}\right) \qquad (4)$$

The gas density is determined from the ideal gas equation of state. The properties of N_2 are determined from kinetic theory expressions through the CHEMKIN computer code (Kee et al. [18], [19]). Equations (1)-(4) are for variable property flow and heat transfer; however, the cases presented in this work are for small temperature differences (maximum 15 K), and the effect of variable properties is primarily in the density changes in the gravitational term (2nd term on the rhs in equation (2)). Reference quantities for nondimensionalization are: channel width, w^*; average inlet flow velocity u^*_{avg}; temperature difference $(T^*_{\mathrm{s}}-T^*_{\mathrm{in}})$, where $T=(T^*-T^*_{\mathrm{in}})/(T^*_{\mathrm{s}}-T^*_{\mathrm{in}})$; and properties evaluated at the inlet temperature, T^*_{in}. The dimensionless parameters in the above equations are the Grashof number $\mathrm{Gr}=g(T^*_{\mathrm{s}}-T^*_{\mathrm{in}})\,\mathrm{w}^{*3}/(T^*_{\mathrm{in}}\,\nu^{*2}_{\mathrm{in}})$, the Reynolds number $\mathrm{Re}=u^*_{\mathrm{in}}\,\mathrm{w}^*/\nu^*_{\mathrm{in}}$, and the Prandtl number $\mathrm{Pr}=c^*_{p_{\mathrm{in}}}\,\mu^*_{\mathrm{in}}/k^*_{\mathrm{in}}$.

The boundary conditions are (for $t>0$):

at $x=-4.3$, for $0\le y\le 1$: $T=0$, $u=6y(1-y)$, $v=0$;

at $y=0$ and 1, for $-4.3\le x<0$: $T=0$, $u=0$, $v=0$;

at $y=0$ and 1, for $0\le x<8.6$: $T=1$, $u=0$, $v=0$;

at $y=0$ and 1, for $8.6\le x\le 52.9$: $\partial T/\partial y=0$, $u=0$, $v=0$;

at $x=52.9$, for $0\le y\le 1$: $\partial T/\partial x=\partial u/\partial x=\partial v/\partial x=0$.

The initial conditions are:

at $t=0$, for $0\le y\le 1$ and for $-4.3\le x\le 52.9$: $T=0$, $u=6y(1-y)$, $v=0$.

Numerical Solution

The conservation equations (1)-(4) were integrated over control volumes and discretized using the hybrid differencing scheme (Patankar [20]). The continuity equation was used in the

SIMPLER method to determine the pressure, p_m. The time derivatives were discretized using the backward Euler method. A sequential line by line relaxation iterative method was applied to solve the discretized equations and boundary conditions. The results shown here were determined using 205 x grids and 34 y grids, with 50 x grids in the heated zone. The grid spacing was nonuniform and finer near the surfaces and the start of the heated region (at x=0). The time step was uniform (Δt=0.0357) for all the results shown.

Convergence criteria

An iterative method was used to solve the coupled, nonlinear set of equations at each time step. Underrelaxation factors (typical values were 0.05 to 0.5) were used for the momentum and energy conservation equations to avoid numerical instabilities; no underrelaxation was applied to the pressure and the pressure correction equations. The convergence criteria were set as follows: iterations within a time step were continued until the relative changes of all variables at all control volumes from one iteration to the next were less than 10^{-4} or until a preset maximum number of iterations (typically 200-300) had occurred. For Gr/Re^2= 1.83, after the initial transient disturbances (which lasted until $t \geq 100$, approximately) subsided, about 60-70 iterations were required per time step. Global mass balances in the channel were satisfied to better than 1%.

Grid and Time Step Sensitivities

The number of grids in the y direction was varied from 26 to 42 and the number of grids in the x direction within the heated region was varied from 38 to 60 for Gr/Re^2=8. Significant differences existed between results obtained using a 50x26 (x,y) grid in the heated region compared with results from a 50x34 grid. However, comparing results from a 50x42 grid with the 50x34 grid showed good agreement for all quantities (within 1-3%; a maximum difference of 5% occurred in the peak value of the local Nusselt number). Comparisons made between results computed on 50x34 and 60x34 grids in the heated region showed agreement to within 1-5% depending on the quantities compared (magnitude and frequency of the oscillations of velocity, temperature, and average and local Nusselt numbers). As a result, the 50x34 grid in the heated region was used.

The time step, Δt, was varied from 0.01785 to 0.14286; for Gr/Re^2=1.83, results of calculations with Δt=0.07143 and 0.0357 agreed to better than 1%; however, for Gr/Re^2=8.0, significant differences were noted for results calculated at these two time steps. A subsequent calculation using Δt=0.01785 showed good agreement with the Δt=0.0357 results (within

1-3% for all quantities except a maximum difference of 5% in the magnitude of one of the local Nusselt number peak values). For Gr/Re^2=13.7, the results at Δt=0.0357 agreed with those obtained at 0.01785 to within 2-4%. The time step, Δt=0.0357, was used for the results discussed below.

RESULTS

Nitrogen enters a vertical channel at $x_{in} = x^*/w^* = -4.3$ (Fig. 1) and flows downward with an inlet temperature T^*_{in} = 300 K (T=0) and an inlet parabolic velocity profile with an average velocity u^*_{avg}=5 cm/s (u=1) corresponding to Re=219.7. In the region near the inlet (from x=−4.3 to x=0) the channel is maintained at the inlet gas temperature (300 K, T=0); from x=0 to x=8.6 the channel temperature is T^*_s(T_s=1); and from x=8.6 to the exit at x=52.9 the channel walls are adiabatic. Figure 2 shows the flow pattern (marker pathline traces for 8 time steps) and the temperature field (the lead arrow of the fluid pathline traces corresponds to the time of the temperature field) in the heated region of the channel for Re=219.7 and Gr/Re^2=13.7; the features shown are characteristic of all three cases discussed later. In the heated zone, the fluid near the wall rises due to buoyancy which opposes the downward flow in the center of the channel. Just upstream of the start of the heated region, the downward flow (cf. white arrows in Fig. 2), which has a parabolic profile at the inlet of the channel, is constricted by the upward buoyant flows near the walls. As the downward flow enters the heated region it accelerates due to the effects of the temperature increase and the upward buoyant flows near the walls. The distance between arrowheads on the pathline traces is directly proportional to the speed of the gas flow. When the upward buoyant flow reaches the top of the heated region and encounters the cooler upper region, it turns toward the centerline and is incorporated into the rapidly moving downward flow in the central core of the channel. This phenomenon occurs periodically and alternately on the two surfaces. The resulting velocity and temperature fields are complex, asymmetric with respect to the centerline of the channel, and periodic.

The first case considered is for T^*_s=302 K corresponding to Gr/Re^2=1.83. The color shaded contours of the temperature and velocity fields are shown in Figs. 3a-f and are clearly not symmetric about the centerline of the channel although the problem specified is symmetric. The results are periodic and the fields are shown at t=251.8 and half a period later at t=259.3. The time t=251.8 corresponds to a minimum temperature at the location x=3.6, y=0.19. Although the fields are nonsymmetric, half a period later Figs. 3a-d show there is a symmetric reflection about the centerline of the channel (of this nonsymmetric field).

Figure 2. Temperature field at one instant of time and selected fluid pathlines (markers show the flow patterns over 8 time steps) in the heated region for Re=219.7, Gr/Re^2=13.7.

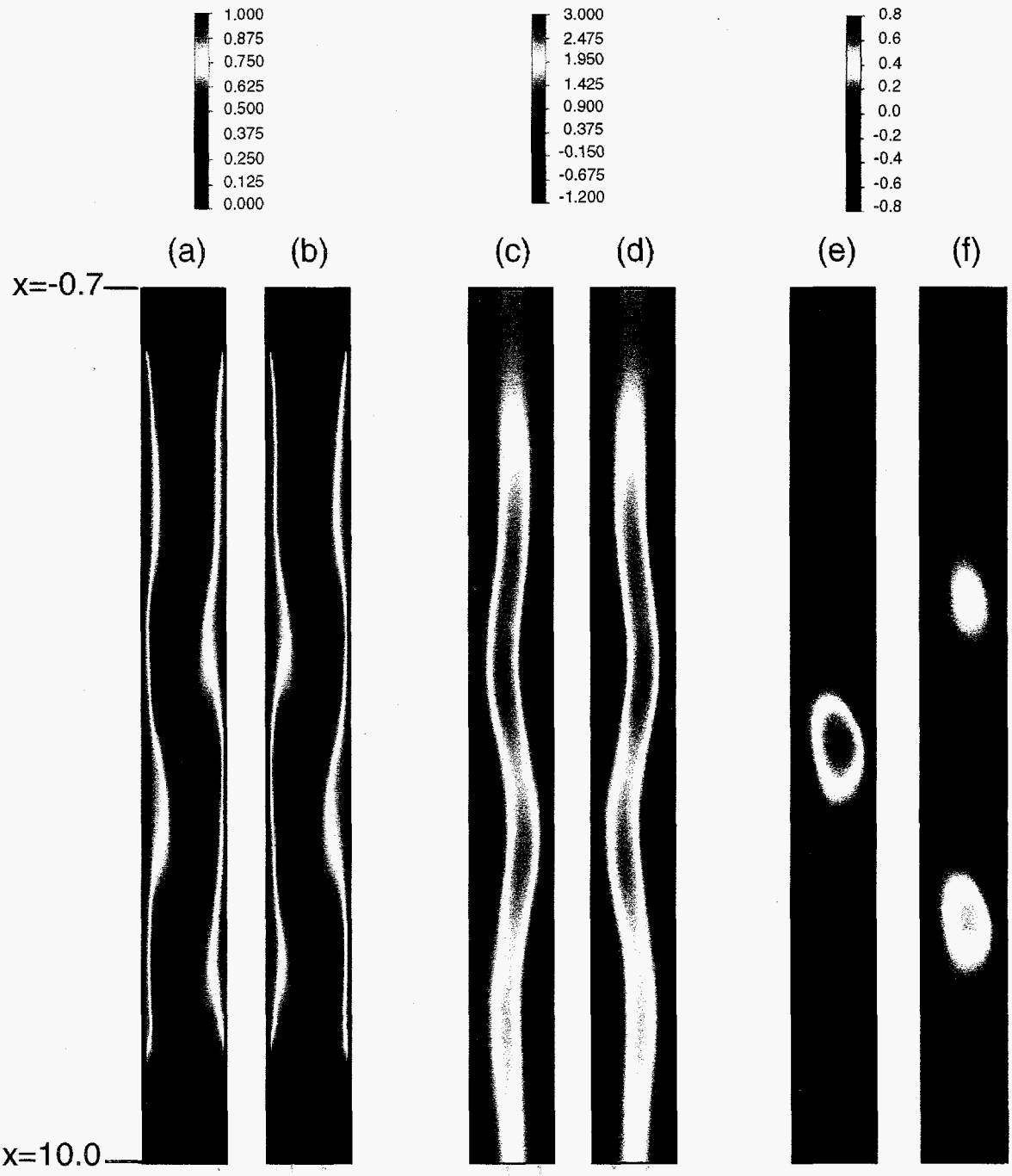

Figure 3. Temperature and velocity fields at t=251.8 (when T is minimum at x= 3.6, y= 0.19) [(a),(c),(e)] and half a period later at t= 259.3 [(b),(d),(f)]; (a),(b) T; (c),(d) u; (e),(f) v; Re=219.7, $\mathrm{Gr/Re^2}$=1.83.

Note that the lateral component of the velocity, v, shows an *antisymmetric* reflection about the centerline (cf. Figs. 3e,f).

Figs. 4a-c show the periodic nature of the temperature and velocity at two axial locations (x=0.7, 3.6) within the heated zone. The temperature, T, and axial component of velocity, u, are shown near one of the channel walls at y=0.19; in addition, the lateral velocity component, v, is also shown near the channel centerline at y=0.47. The amplitudes of all the oscillations are largest near the central part of the heated zone (x=3.6 curves). The periodic flow also exhibits flow reversals (u positive and negative in Fig. 4b); v also takes on positive and negative values (Fig. 4c). A power spectral analysis of the oscillations of the velocity and temperature at selected points using 2048 time steps yields a single period of 15 (frequency of 0.07). For symmetric flows v would be zero at the centerline; here there are large oscillations in v near the centerline which disturb the symmetry of the flow. The oscillations can have a deleterious effect on some processes; e.g., fiber drying, reactor cooling, ventilation, food processing, etc.

Lateral profiles of T, u, and v are shown at two times (t=251.8 and 259.3) for different axial positions in Figs. 5a-c (as stated above, the results are not symmetric about the centerline of the channel). Recall that the time t=251.8 corresponds to a minimum temperature at x=3.6, y=0.19. The upward buoyant flow near the wall does not penetrate upstream into the unheated region (x<0) as shown by the parabolic profile for u (Fig. 5b). Figure 5b shows that the buoyant upflow along the channel walls in the heated zone results in an enhanced maximum value of u ($u_{\max}$=2.5 at x=3.6). Comparisons of curves at the same axial location x having the same symbols at times that are one-half of a period apart show that both T and u are symmetric about the centerline half a period later (Figs. 5a,b), whereas v is antisymmetric about the centerline half a period later (Fig. 5c).

Axial variations (which complement the lateral variations of Figure 5) of temperature and velocity close to and equidistant from both side walls of the channel (y=0.19 and 0.81) are shown in Figs. 6a-c at t=251.8 and 259.3. Both T and u clearly exhibit two maxima which are also seen in Figure 3. Comparisons of T and u at y=0.19, t=251.8 and at y=0.81, t=259.3 overlap, showing symmetry about the centerline half a period later; v shows antisymmetry about the centerline half a period later; these reflections in time and space are also seen in Figure 3.

The axial profiles of temperature and velocity along the channel centerline are shown in Figs. 7a-c at t=251.8 and t=259.3. In contrast to the stronger upward buoyant region near

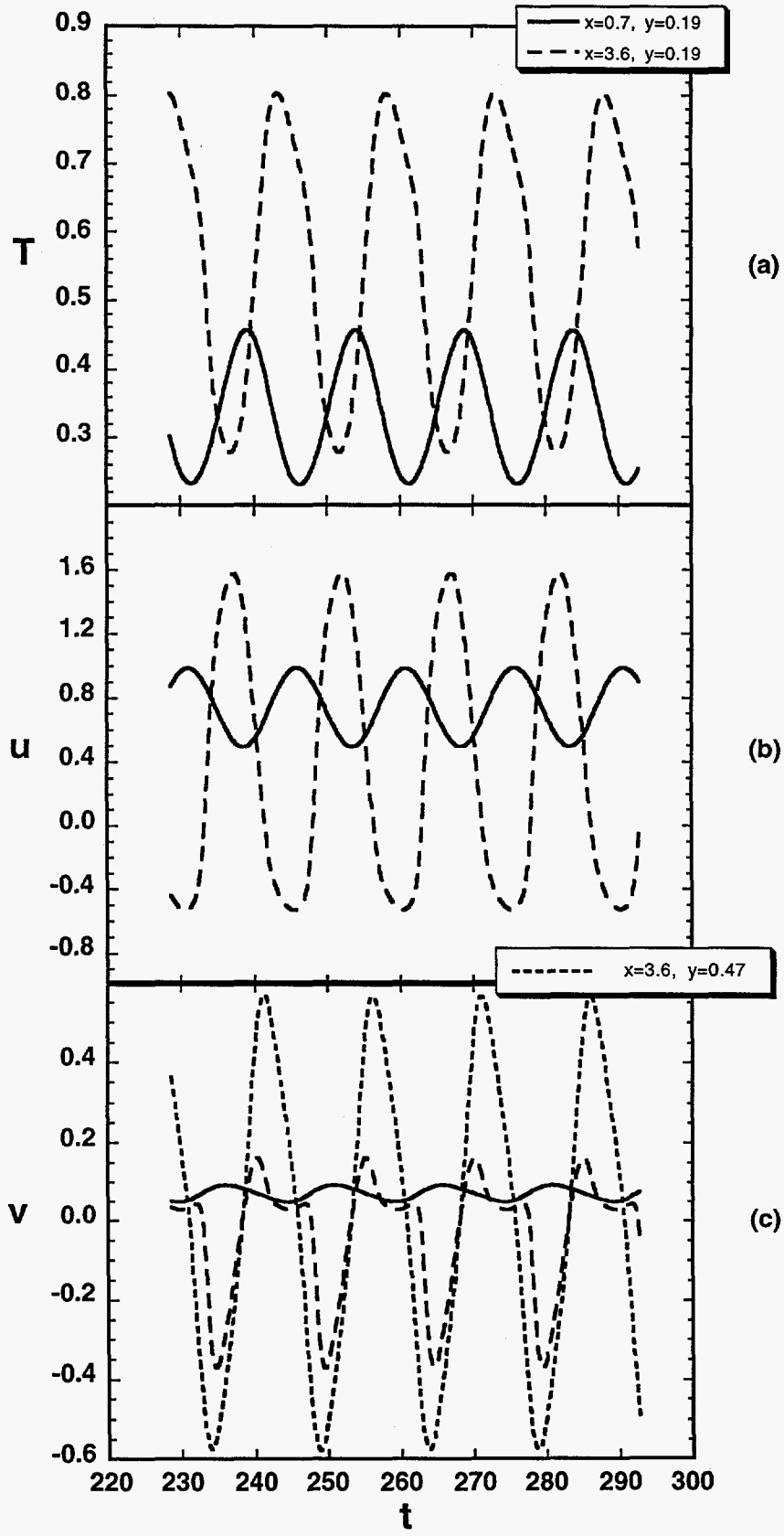

Figure 4. Time variations of temperature (a) and velocity (b,c) at y= 0.19, 0.47 and x= 0.7, 3.6; Re=219.7, Gr/Re^2=1.83.

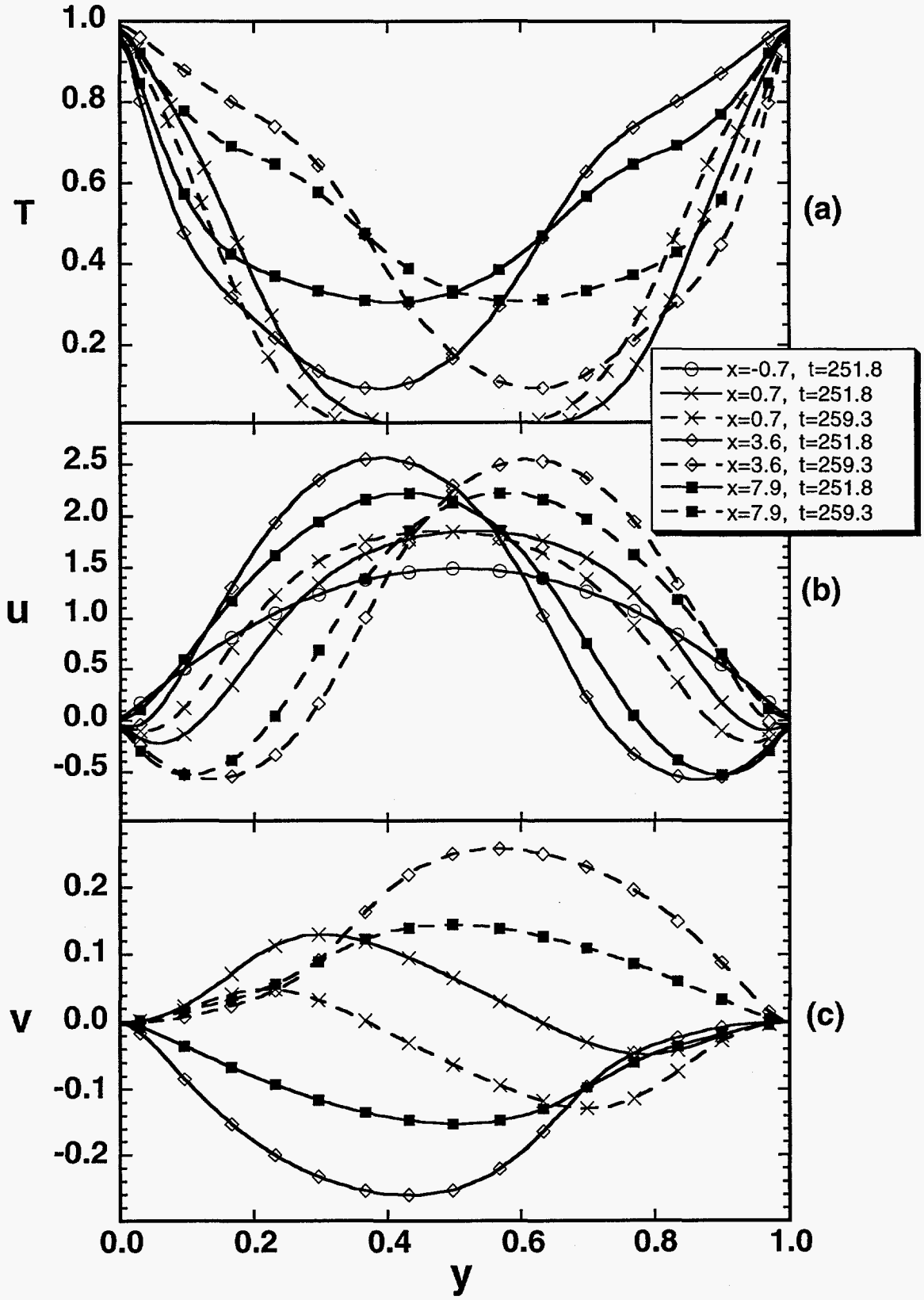

Figure 5. Lateral variations of temperature (a) and velocity (b,c) at two times (t= 251.8 and 259.3) half a period apart; Re=219.7, Gr/Re^2=1.83.

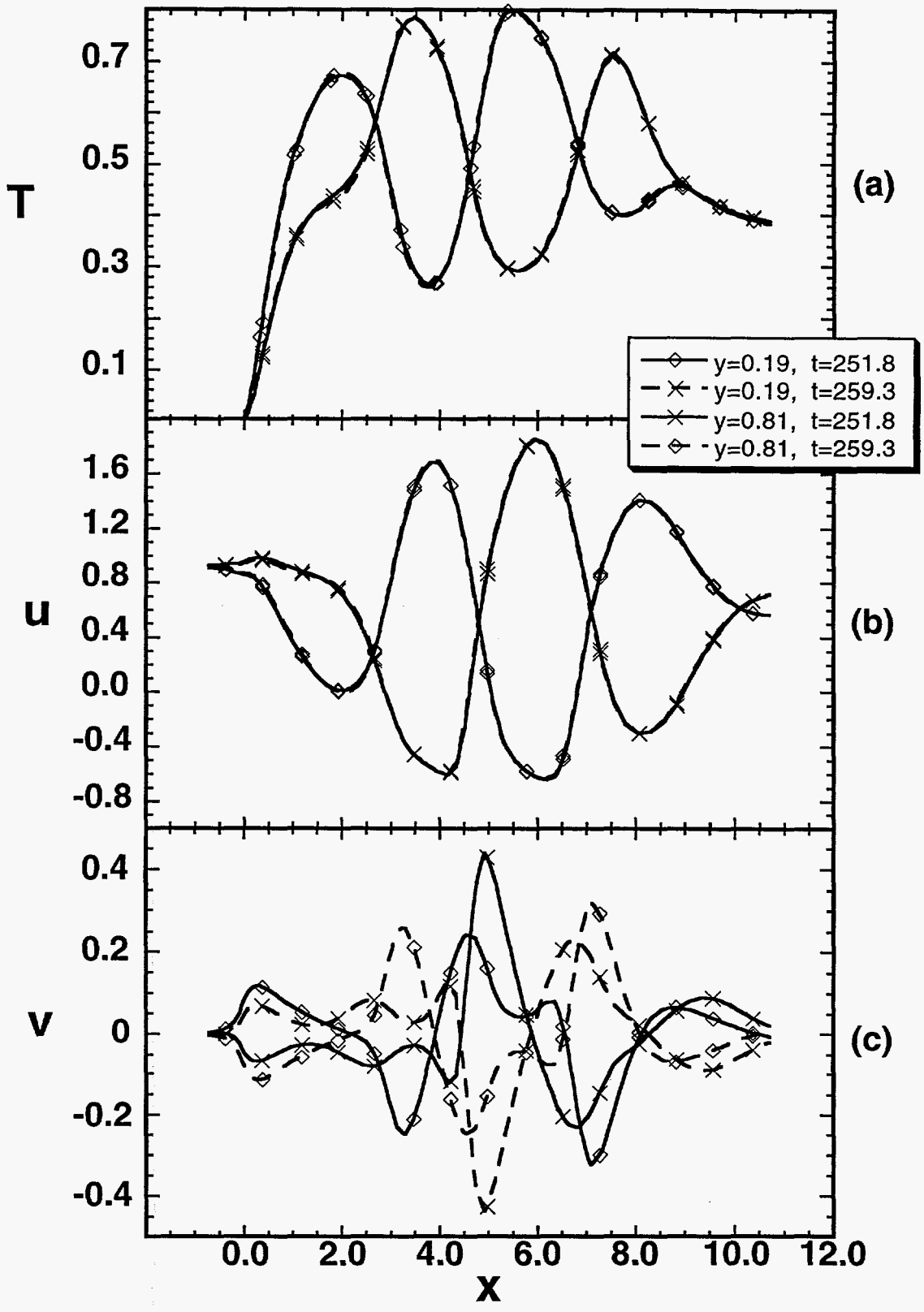

Figure 6. Axial variations of temperature (a) and velocity (b,c) at two times (t= 251.8 and 259.3) half a period apart; Re=219.7, Gr/Re^2=1.83.

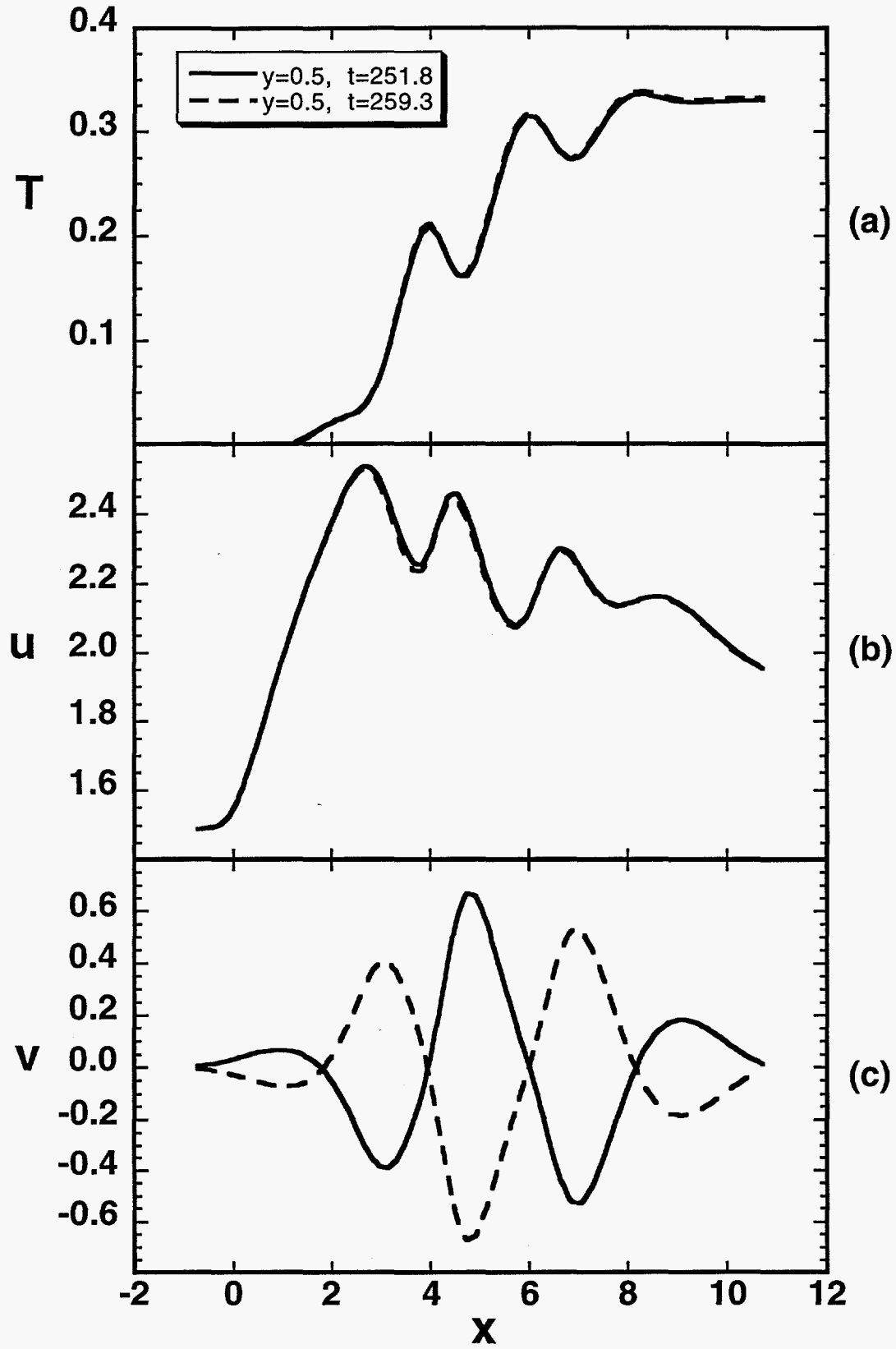

Figure 7. Axial variations of temperature (a) and velocity (b,c) along the channel centerline at two times (t= 251.8 and 259.3) half a period apart; Re=219.7, Gr/Re^2=1.83.

the wall where the flow is both upward (u <0) and downward (u >0) as shown in Fig. 6b, u at the centerline is always downward with alternating maxima and minima. At the centerline T also has alternating maxima and minima; v exhibits positive and negative values at the centerline as shown in Fig. 7c (also see Fig. 4c) and near the walls (Fig. 6c). Identical profiles of T and u occur half a period apart while the profile of v is "opposite" half a period later.

The average Nusselt numbers shown in Figure 8a show a periodic oscillation which exhibits a higher frequency component which is also present in the v velocity component in Fig. 4c. The time average of $\mathrm{Nu_{avg}}$ is approximately 3.7. The local Nusselt numbers shown in Fig. 8b at t=251.8 exhibit nonmonotonic variations.

The effects of increasing $\mathrm{Gr/Re^2}$for fixed Re=219.7 are shown in Figure 9 where the fields of T, u, and v are shown for $\mathrm{Gr/Re^2}$=1.83, 8.0 and 13.7. The three cases are shown at times when the temperature is a minimum at the location x=3.6, y=0.19. For increasing buoyancy there are stronger oscillations and a more pronounced effect near the start of the heated zone, x=0. However, even for the large values of the mixed convection parameter there is little penetration of the heated, buoyant fluid upstream of the heated zone, x<0 (for the cold isothermal boundary condition considered in this study where $T_s = T_{\mathrm{in}}$ for $-4.3 \leq x < 0$).

The period of the oscillations decreases from 15.0 to 3.8 to 3.0 (frequency increases from 0.07 to 0.26 to 0.33) with increasing $\mathrm{Gr/Re^2}$. The complexity and amplitudes of the oscillations has increased significantly from the simpler variations at lower buoyancy (cf. Fig. 4) and are shown in Figure 10 for the case $\mathrm{Gr/Re^2}$=13.7. Note the increased amplitudes of T and v near the start of the heated region (x=0.7). For this case, a spectral analysis of the temperature oscillations shows small components at two and three times the fundamental frequency of 0.33. Temperature oscillations with frequencies ranging from 0.003 to 0.1 in opposed flow mixed convection for different thermal boundary conditions (13, 17) and in tube flow (16) have been reported in the literature.

Lateral profiles similar to Figure 5 were also obtained at the higher values of Gr (not shown). These results show increased heating in the center of the channel and larger positive and negative values of both axial and lateral components of velocity, especially near the start of the heated region. Axial profiles of T, u, and v near the walls at higher buoyancy ($\mathrm{Gr/Re^2}$=13.7 in Fig. 11) show greater spatial variation and clearly exhibit the symmetric (T and u) and antisymmetric (v) reflections that were previously noted for lower buoyancy.

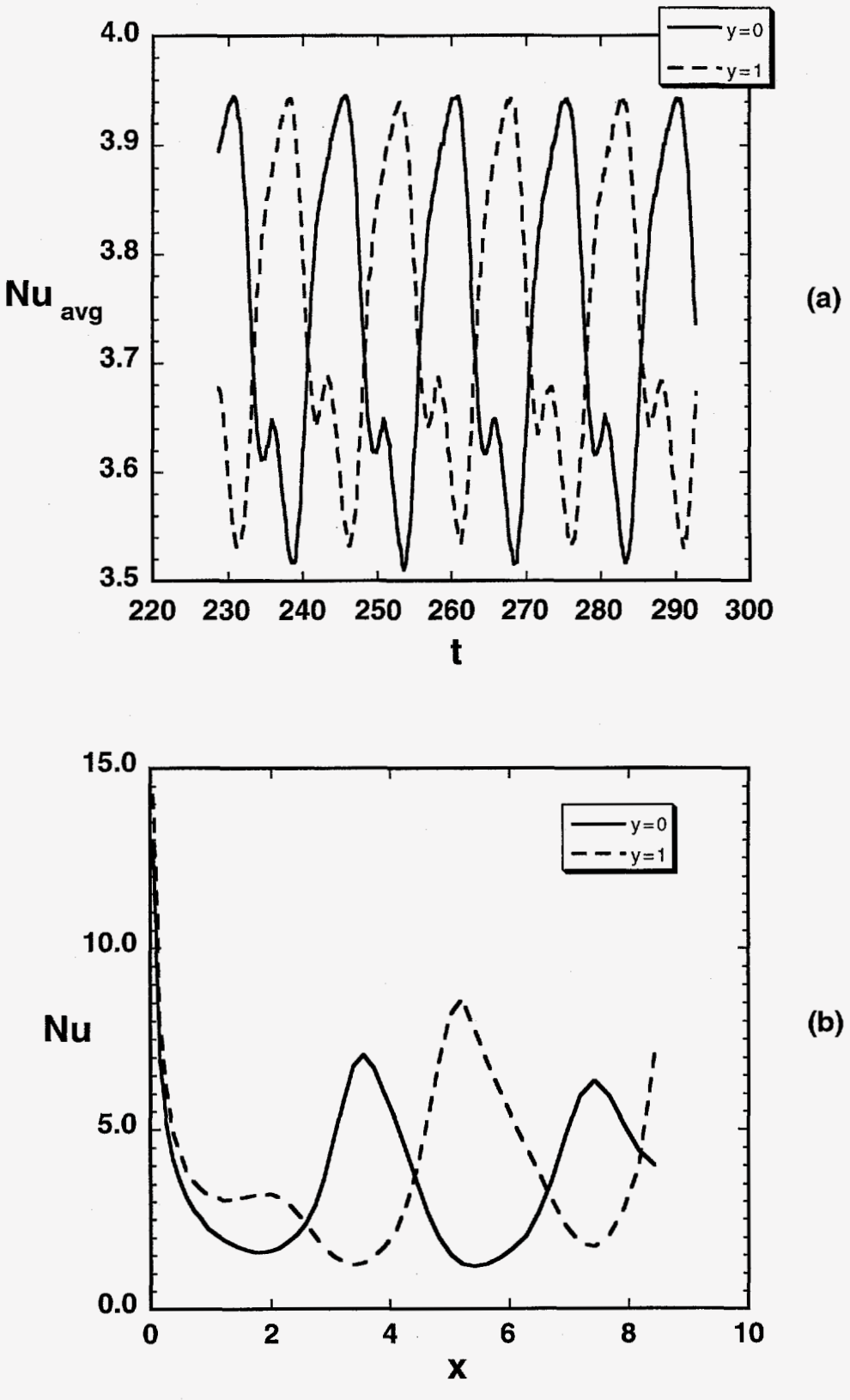

Figure 8. Heat transfer from channel surfaces; (a) average Nusselt numbers; (b) local Nusselt numbers at t= 251.8; Re=219.7, Gr/Re^2=1.83.

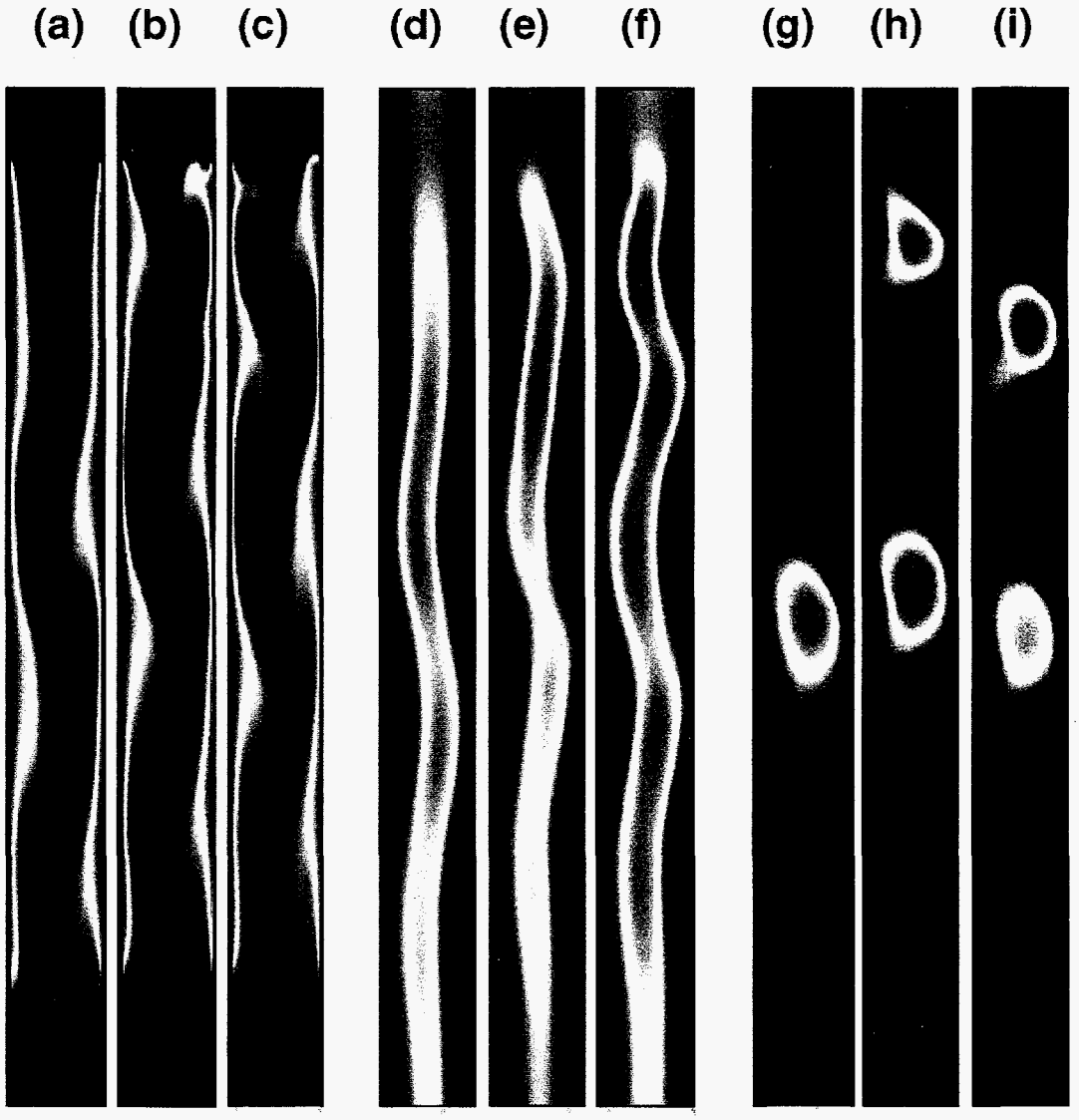

Figure 9. Temperature and velocity fields at times when T is minimum at x= 3.6, y= 0.19 for Re = 219.7 and three values of Gr; (a),(d),(g): $\mathrm{Gr/Re^2}$= 1.83; (b),(e),(h): $\mathrm{Gr/Re^2}$= 8.0; (c),(f),(i): $\mathrm{Gr/Re^2}$= 13.7; (a)-(c): T; (d)-(f): u; (g)-(i): v.

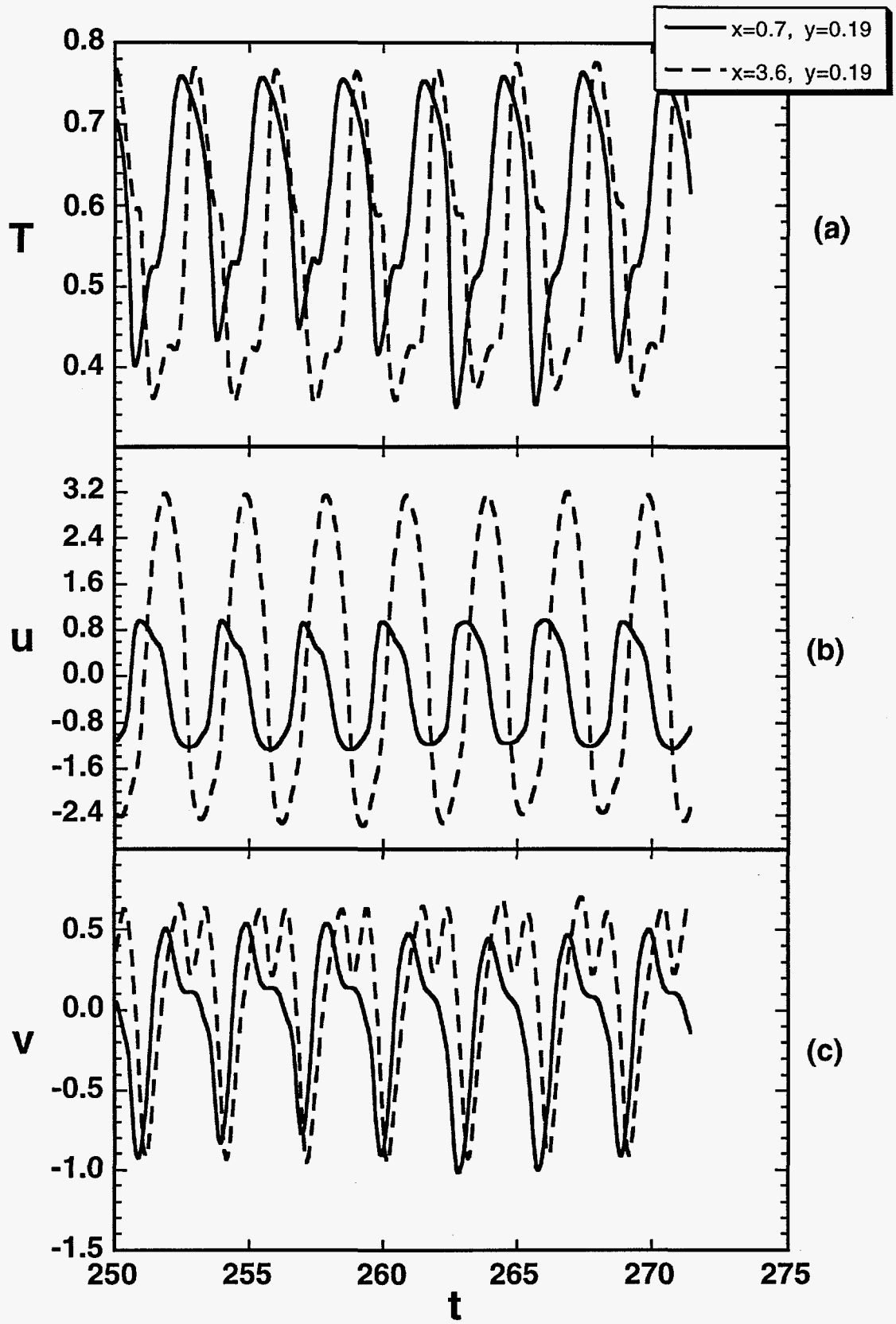

Figure 10. Time variations of temperature (a) and velocity (b,c) at y= 0.19 and x= 0.7, 3.6; Re=219.7, Gr/Re^2=13.7.

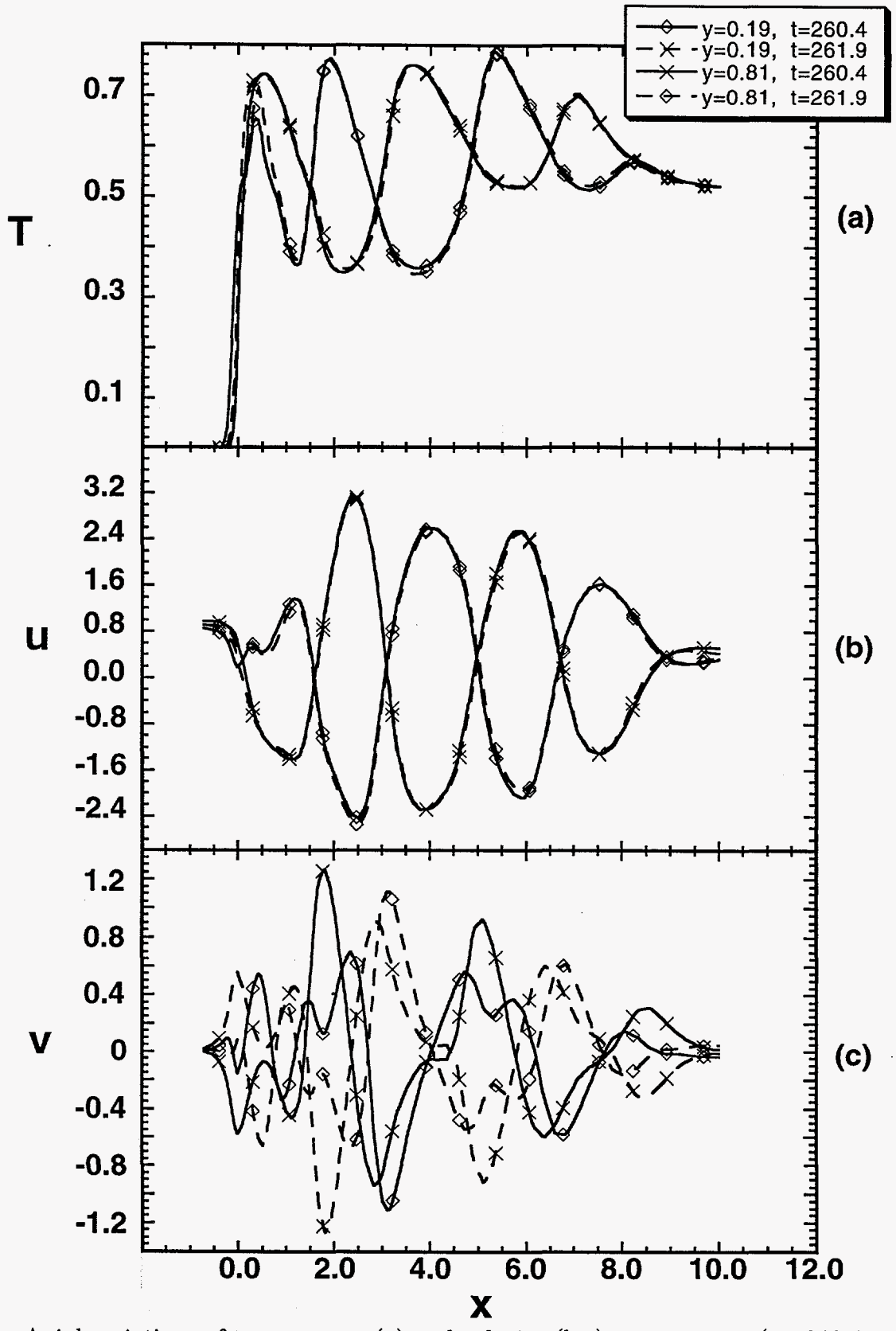

Figure 11. Axial variations of temperature (a) and velocity (b,c) at two times (t= 260.4 and 261.9) half a period apart; Re=219.7, Gr/Re^2=13.7.

For increasing buoyancy (Gr/Re^2=1.83, 8.0, 13.7) the time average of Nu_{avg} increases from 3.7 to 4.5 to 4.9, approximately; the Gr/Re^2=13.7 case is shown in Fig. 12 which also includes the local Nusselt number. There is an increased heat transfer near the start of the heated region (cf. Figs. 12b and 8b). We note that the above results for these time averaged Nusselt numbers are similar to those reported in other studies involving mixed convection; increasing heat transfer with increasing buoyancy has been observed although there is some evidence of a limited region of reduced heat transfer with increasing buoyancy in opposed mixed convection flow in converging channels with constant heat flux boundary conditions (17).

CONCLUSIONS

Unsteady, two-dimensional simulations of the downward flow of N_2 in a vertical heated (isothermal) channel with an upstream cold section show the importance of buoyancy. Results for the temperature, velocity, and heat transfer have been obtained for Re=219.7, Pr=0.7, and Gr/Re^2=1.83, 8.0, and 13.7. To minimize property variations the temperature differences were small; i.e., 2, 8.7, and 15 degrees Kelvin for the three cases, respectively. For all cases there is an upward buoyant flow near the walls that turns downward at the top of the heated section. Near the walls, the axial flow reverses direction periodically; the lateral flow reverses direction both at the centerline and near the walls. The temperature and axial component of velocity along the centerline of the channel are nonmonotonic and oscillatory. The results are nonsymmetric, periodic, and exhibit increasing complexity and frequency for increasing buoyancy. The temperature and axial component of velocity half a period apart show symmetric reflections (of the asymmetric fields) while the lateral component of velocity, v, shows antisymmetric reflections. The average heat transfer is periodic and increases with increasing buoyancy.

Acknowledgements— The authors would like to thank Chris Shelton, Glen Connell, and Margaret Vogel-Martin of the 3M company for sharing their data with us and for several valuable discussions. This work was supported by the U.S. Department of Defense (DARPA-DSO), Order No. 8951DPAM21264, and the U.S. Department of Energy, Contract DE-AC04-94-AL85000. The DARPA monitor was William Barker.

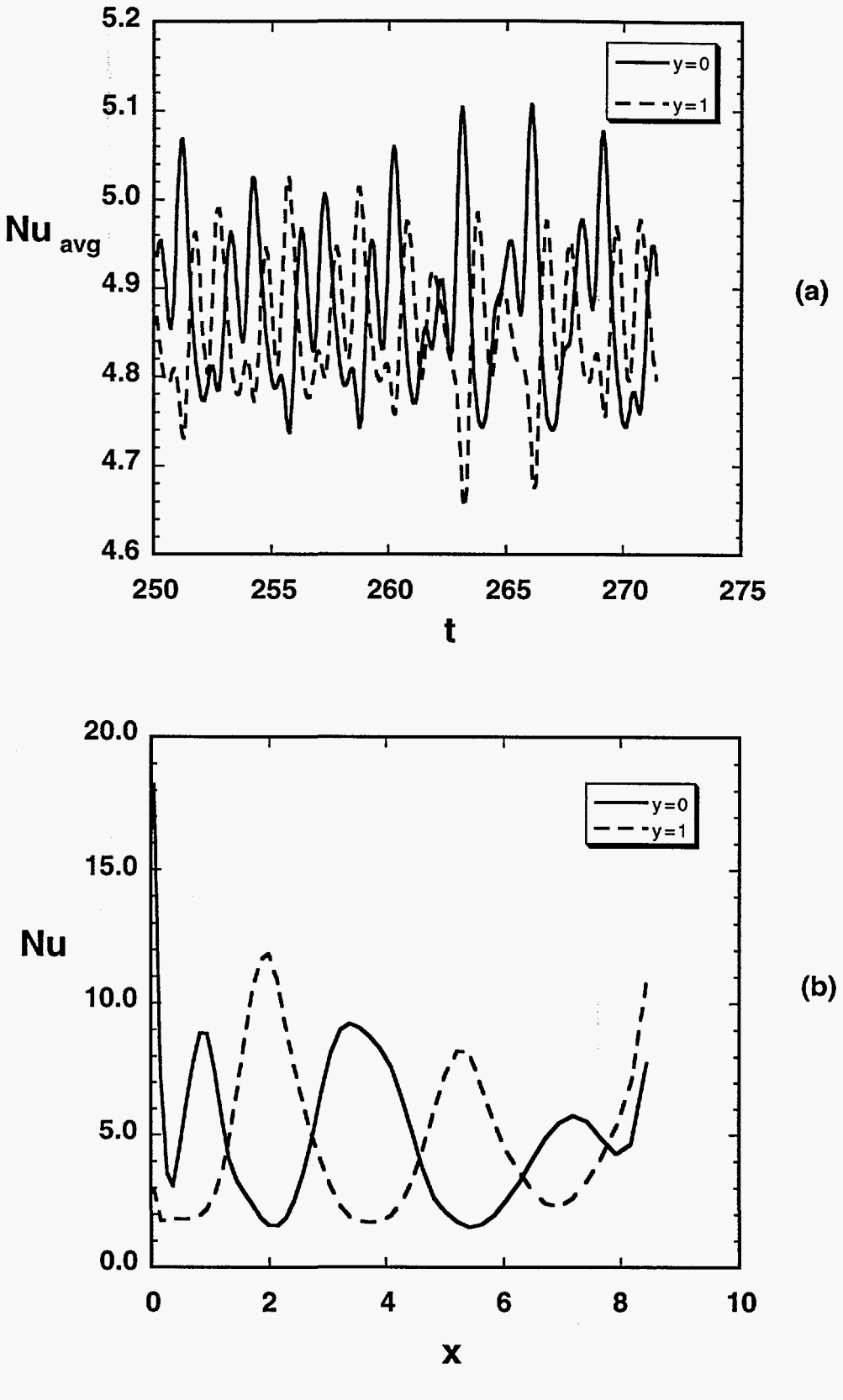

Figure 12. Heat transfer from channel surfaces; (a) average Nusselt numbers; (b) local Nusselt numbers at t= 260.4; Re=219.7, Gr/Re^2=13.7.

REFERENCES

1. S. Ostrach, Combined Natural- and Forced-Convection Laminar Flow Heat Transfer of Fluids with and without Heat Sources in Channels with Linearly Varying Wall Temperatures, *NACA TN 3141*, (1954).

2. B. R. Morton, Laminar Convection in Uniformly Heated Vertical Pipes, *J. Fluid Mech.* **8,** 227-240 (1960).

3. G. F. Scheele and T. J. Hanratty, Effects of Natural Convection on Stability of Flow in a Vertical Pipe, *J. Fluid Mech.* **14,** 244-256 (1962).

4. W. T. Lawrence and J. C. Chato, Heat-Transfer Effects on the Developing Laminar Flow inside Vertical Tubes, *J. Heat Transfer* **88,** 214-222 (1966).

5. B. Zeldin and F. W. Schmidt, Developing Flow with Combined Free-Forced Convection in an Isothermal Vertical Tube, *J. Heat Transfer* **94,** 211-223 (1972).

6. J. Quintiere and W. K. Mueller, An Analysis of Laminar Free and Forced Convection between Finite Vertical Parallel Plates, *J. Heat Transfer* **95,** 53-59 (1973).

7. T. Cebeci, A. A. Khattab, and R. LaMont, Combined Natural and Forced Convection in Vertical Ducts, *Proceedings of 7th Int. Heat Transfer Conf.; Munich, Germany* **1,** 419-424 (1982).

8. L. S. Yao, Free and Forced Convection in the Entry Region of a Heated Vertical Channel, *Int. J. Heat Mass Transfer* **26,** 65-72 (1983).

9. M. A. Shadday, Jr., Combined Forced/Free Convection through Vertical Tubes at high Grashoff Numbers, *Proceedings of 8th Int. Heat Transfer Conf.; San Francisco, CA* **3,** 1433-1437 (1986).

10. S. Habchi and S. Acharya, Laminar Mixed Convection in a Symmetrically or Asymmetrically Heated Vertical Channel, *Numerical Heat Transfer* **9,** 605-618 (1986).

11. M. Wang, T. Tsuji, and Y. Nagano, Mixed Convection with Flow Reversal in the Thermal Entrance Region of Horizontal and Vertical Pipes, *Int. J. Heat Mass Transfer* **37,** 2305-2319 (1994).

12. T. S. Chang and T. F. Lin, Steady and Oscillatory Opposing Mixed Convection in a Symmetrically Heated Vertical Channel with a Low-Prandtl Number Fluid, *Int. J. Heat Mass Transfer* **36,** 3783-3795 (1993).

13. T. F. Lin, T. S. Chang, and Y. F. Chen, Development of Oscillatory Asymmetric Recirculating Flow in Transient Laminar Opposing Mixed Convection in a Symmetrically Heated

Vertical Channel, *J. Heat Transfer* **115,** 342-352 (1993).

14. H. N. Guerrero and C. M. Hart, Flow Instability and Flow Reversal in Heated Annular Multichannels with Initial Downward Flow, *Proceedings Nat. Heat Transfer Conf.* (1993).

15. B. B. Rogers and L. S. Yao, Finite-amplitude Instability of Mixed Convection in a Heated Vertical Pipe, *Int. J. Heat Mass Transfer* **36,** 2305-2315 (1993).

16. D. D. Joye and S. W. Jacobs, Backflow in the Inlet Region of Opposing Mixed Convection Heat Transfer in a Vertical Tube, *Proceedings of 10th Int. Heat Transfer Conf.; Brighton, UK* **5,** 489-494 (1994).

17. C. Gau, T. M. Huang, and W. Aung, Mixed Convection Flow and Heat Transfer in a Heated Vertical Convergent Channel, *paper AIAA 94-2012, 6th AIAA/ASME Joint Thermophysics and Heat Transfer Conf.; Colorado Springs, CO* (1994).

18. R. J. Kee, G. Dixon-Lewis, J. Warnatz, M. E. Coltrin, and J. A. Miller, A Fortran Computer Code Package for the Evaluation of Gas-Phase Multicomponent Transport Properties, *Sandia Report SAND86-8246* (1986).

19. R. J. Kee, F. M. Rupley, and J. A. Miller, CHEMKIN-II: A Fortran Chemical Kinetics Package for the Analysis of Gas-Phase Chemical Kinetics, *Sandia Report SAND89-8009* (1989).

20. S. V. Patankar, *Numerical Heat Transfer and Fluid Flow*, McGraw-Hill (1980).

UNLIMITED RELEASE
INITIAL DISTRIBUTION

C. E. Shelton
3M Industrial and Electronics Sector
Building 60-1N-01
St. Paul, MN 55144-1000

G. Connell
3M Industrial and Electronics Sector
Building 60-1N-01
St. Paul, MN 55144-1000

M. Vogel-Martin
3M Industrial and Electronics Sector
Building 60-1N-01
St. Paul, MN 55144-1000

R. Greif (5)
Mechanical Engineering Dept.
University of California at Berkeley
Berkeley, CA 94720-1740

O. A. Plumb
Mechanical and Materials Engineering Dept.
Washington State University
Pullman, WN 99164

S. Paolucci
Aerospace and Mechanical Engineering Dept.
University of Notre Dame
Notre Dame, IN 46556

R. Mahajan
Mechanical Engineering Dept.
University of Colorado
Boulder, CO 80309

F. P. Incropera
Mechanical Engineering Dept.
Purdue University
West Lafayette, IN 47907

W. Richter
Berlin University of Technology
Institute of Solid State Physics
Sekr. PN 6-1
Berlin, Germany

C. R. Kleijn
Delft University of Technology
Faculty of Applied Physics
Kramers Laboratorium voor Fysische Technologie
Prins Bernhardlaan 6
2628 BW Delft, The Netherlands

R. E. Kelly
Mechanical and Aerospace Engineering Dept.
School of Engineering and Applied Science
405 Hilgard Ave.
University of California, Los Angeles
Los Angeles, CA 90024-1597

A. Lavine
Mechanical and Aerospace Engineering Dept.
School of Engineering and Applied Science
405 Hilgard Ave.
University of California at Los Angeles
Los Angeles, CA 90024-1597

D. D. Joye
Chemical Engineering Dept.
Villanova University
800 Lancaster Ave.
Villanova, PA 19085-1681

R. J. Kee
Engineering Division
Colorado School of Mines
Golden, CO 80401-1887

0601 W. G. Breiland, 1126
0601 H. K. Moffat, 1126
0601 J. Y. Tsao, 1126
9001 T. O. Hunter, 8000
Attn: M. E. John, 8100
A. West, 8200
R. C. Wayne, 8400
A. West, 8600
T. M. Dyer, 8700
L. E. Hiles, 8800
D. L. Crawford, 8900

9054 W. J. McLean, 8300
Attn: C. W. Robinson, 8301
W. Bauer, 8302
L. A. Rahn, 8351
F. P. Tully, 8353
D. R. Hardesty, 8361
R. W. Carling, 8362
R. J. Gallagher, 8366
9042 G. H. Evans, 8345 (10)
9042 S. K. Griffiths, 8345
9042 C. M. Hartwig, 8345
9042 R. S. Larson, 8345
9042 R. H. Nilson, 8345
9051 J. Chen, 8351
9051 H. Najm, 8351
9405 L. A. Bertram, 8743
9042 D. R. Chenoweth, 8743
9042 M. P. Kanouff, 8743
0841 P. J. Hommert, 9100
Attn: R. D. Skocypec, 9102
W. L. Hermina, 9111
A. C. Ratzel, 9112
0826 C. E. Hickox, 9111
0826 P. R. Schunk, 9111
0834 M. R. Baer, 9112
9021 Tech. Communications Dept., 8515
for OSTI (10)
9021 Tech. Communications, 8815
0899 Tech. Library, 4414 (4)
9018 Central Tech. Files, 8940-2 (3)